Single-crystal Mössbauer measurement of the critical exponent β in the random-exchange Ising system $Fe_{0.9}Zn_{0.1}F_2$

N. Rosov, A. Kleinhammes, P. Lidbjörk, and C. Hohenemser
Department of Physics, Clark University, Worcester, Massachusetts 01610

M. Eibschütz
AT&T Bell Laboratories, Murray Hill, New Jersey 07974
(Received 28 August 1987)

Mössbauer measurements of the hyperfine field, $H_{hf}(T)$, for the random-exchange Ising system $Fe_{0.9}Zn_{0.1}F_2$ are reported for the critical region. Concentration gradients were minimized by choosing a single crystal with its growth axis perpendicular to the plane of the absorber. Inhomogeneous broadening was treated by fitting with four magnetic sites, using a procedure that explicitly diagonalizes the Hamiltonian. This indicates that residual short-range order is negligible, demonstrates that H_{hf} is aligned with a principal axis of the electric-field gradient, and gives excellent fits. Rounding of the transition was determined via constant-velocity thermal scanning, and implies that residual concentration variability was <0.03 at. %. After corrections to scaling, the data yield a critical exponent $\beta=0.350(9)$ in the reduced-temperature range of $3\times10^{-4}<t<10^{-1}$. This result is consistent with the most recent theoretical prediction, $\beta=0.3494(15)$.

I. INTRODUCTION

The role of randomness in critical behavior continues to be of considerable interest. Particular foci are the effect of random exchange (RE) and random fields (RF). The RE interaction is described by

$$\mathcal{H}_{RE}=\sum_i\sum_j(J_0+\Delta J_{ij})\mathbf{S}_i\cdot\mathbf{S}_j-\sum_i O_i(\mathbf{S}_i)\ , \qquad (1)$$

where the first sum runs over the constituent atoms and the second over nearest neighbors, J_0 is the average exchange interaction, $\mathbf{S}_i$ is the m-component spin, ΔJ_{ij} is the random exchange variable, and $O_i(\mathbf{S}_i)$ is a single ion anisotropy term allowed by the symmetry of the crystal. The RF interaction involves the addition of a Zeeman term, $\sum_i h_i S_i$, where h_i is a site random field.[1]

There was no convenient realization of a RF system until Fishman and Aharony[2] showed that a RE *Ising antiferromagnet* with a magnetic field, H_a, applied along the easy axis is equivalent to a *Ising ferromagnet* in which each ion is subject to a random field, h_i. This system is known as the random-field Ising model (RFIM). Compared to the pure Ising model, the RFIM is predicted to have drastically altered critical behavior.

Whereas considerable experimental progress has been made on the $d=3$ RFIM,[3] there are still no reliable results for the magnetization below T_c. An excellent candidate for such a measurement is a Mössbauer spectroscopy (MS) study of $Fe_{1-x}Zn_xF_2$.

A first step in a MS investigation of the RFIM below T_c must be a study of the RE Ising model (REIM), i.e., a zero-field measurement. Such a measurement is itself of intrinsic interest since the REIM is the only case for which RE exponents are expected to differ from the pure system.[4,5] In this paper we report on such a measurement, using a single crystal absorber of $Fe_{0.9}Zn_{0.1}F_2$ in which the growth axis, c axis, and γ-ray direction are all collinear and perpendicular to the plane of the disk. Such a sample can reduce concentration gradients to a practical minimum and, once characterized, can be directly used to study RFIM behavior.

Mössbauer spectra were fitted to four magnetic sites, using a procedure that explicitly diagonalizes the Hamiltonian. This provides excellent fits to spectral intensities and line shapes, demonstrates that residual short-range order is negligible, and validates the assumption made by others that H_{hf} is collinear with a principal axis of the electric-field gradient (EFG). A limit on concentration variability was set by measuring T_c rounding via constant-velocity thermal scans.

From the hyperfine field component corresponding to no Zn next nearest neighbors we deduce a critical exponent, $\beta=0.350(9)$, which we believe to be the most reliable experimental value of β for the REIM. It differs significantly from $\beta=0.3250(15)$ expected for the pure Ising model,[6] is in good agreement with the recent prediction[7] $\beta=0.3494(15)$, and encourages us to continue with RFIM studies.

Our agreement with theory is consistent with measurements of other exponents on the REIM.[8,9] Our measurements may be directly compared to the single-crystal NMR study of $Mn_{0.87}Zn_{0.13}F_2$ by Dunlap and Gottlieb[10] and the powder-sample MS study of $Fe_{1-x}Zn_xF_2$, $0.01<x<0.54$, by Barrett.[11] Whereas both yield β values consistent with theory, neither provides an analysis as complete as the present work (see Sec. V below).

II. INSTRUMENTATION

The instrumentation for our study consisted of an Air Products Displex CS-202 closed-cycle He refrigerator with a DMX-20 Mössbauer shroud, an ELSCINT Model MDF-N-5 velocity drive, a 10 mCi ^{57}Co*Pd* single-line source operated at room temperature, and a Reuter Stokes Kr-CO_2 Model RSG-61-M2 proportional counter, coupled to standard electronics.

Temperature control. Absorbers were mounted in a disk-shaped Cu sample holder that was regulated via a two-stage temperature control system of our own design, as illustrated in Fig. 1. The samples were placed in strain-free Lucite pillboxes between two BeO disks and attached with high-thermal-conductivity grease to the sample holder. A 0.7%-Fe*Au*-Constantan thermocouple between one of the BeO disks and the Lucite holder provided an independent temperature measurement. Stability better than ± 3 mK/day was obtained for $10 < T < 80$ K. Temperature uniformity was determined to be less than ± 10 mK over the 0.2 cm^2 area of the absorber by a differential thermocouple.

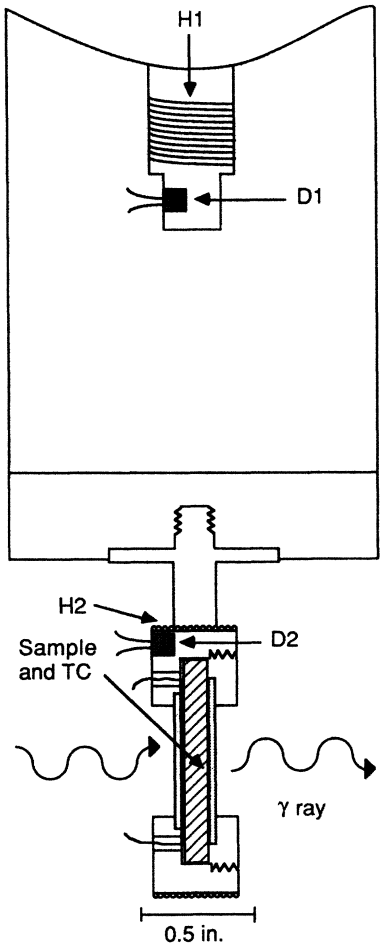

FIG. 1. Cold-finger arrangement with temperature-control system. The primary heater H1 and the diode D1 regulate and measure the temperature of the cold finger connected to the closed-cycle ^{4}He refrigerator. Exchange gas couples the cold finger to the sample holder, which is controlled via a feedback system consisting of the secondary heater H2 and the Si diode D2. A thermocouple TC provides an independent determination of T.

Constant-acceleration spectra. 512-channel constant-acceleration spectra were recorded with an Apple II computer equipped with a multiscaling board designed by Arends.[12] Velocity calibration was accomplished via an Fe absorber. Due to a vibration isolation bellows, residual line broadening caused by the Displex compressor was not detectable. Thus a single-crystal sample of $Fe_{0.9}Zn_{0.1}F_2$ had a linewidth 0.315(4) mm/s at 295 K with the compressor off, and 0.346(4) mm/s at 200 K with the compressor on. Correcting the recoil-free fraction,[13] from $f=0.588$ at 295 K to $f=0.688$ at 200 K,[14] converts the 200 K result to a line width of 0.316(4), indicating almost no vibration broadening.

Constant-velocity scans. To study transition rounding we performed constant-velocity transmission (CVT) thermal scans near T_c with two scalers gated to measure the transmissions, $\tau(-v_0)$ and $\tau(+v_0)$ at two velocities, $\pm v_0$. These were chosen to provide a sharp break at T_c in the temperature dependence of the transmission ratio $\tau(+v_0,T)/\tau(-v_0,T)$.

III. SAMPLE CHARACTERIZATION

A. Magnetic structure

Pure FeF_2, to which our samples are closely related, is one of the best-characterized magnetic systems known. It has a rutile structure with the principal components of the EFG along the two-fold symmetry axes and orders as a strongly anisotropic antiferromagnet below ~ 79 K. In the ordered state the magnetization is along the c axis, which is also the smallest principal component of the EFG.[15]

As indicated in Table I, high-quality measurements of the critical exponents α, β, γ, ν, and z indicate that FeF_2 is a model $d=3$ Ising system. The methods used include specific heat,[16] MS,[17] NMR,[18,19] and neutron scattering,[20,21] and all but some early neutron work[20] yield exponents in excellent agreement with the most recent static[6] and dynamical[22] theory.

ZnF_2 has the same crystal structure as FeF_2 with similar lattice constants and so forms a solid solution with FeF_2 at all concentrations. Based on MS work between 295 K and 4.2 K, Wertheim[23] found that the quadrupole interaction and isomer shift of FeF_2 are unchanged by Zn dilution, but that Zn dilution decreases T_c and the average saturation hyperfine field: viz., $dT_c/dx=-0.78$ K/at. % Zn and $dH_{hf}(0)/dx=-0.545$ kG/at. % Zn. Wertheim used the latter result to explain the degree of inhomogeneous broadening at 4.2 K.

Using methods of analysis described in Sec. IV, we have made a careful comparison of our measurements on $Fe_{0.9}Zn_{0.1}F_2$ and the work of Wertheim.[23] Our findings for $H_{hf}(0)$, dT_c/dx, $dH_{hf}(0)/dx$, center shift, and quadrupole splitting are consistent with Wertheim's findings to within experimental error (see Sec. IV).

TABLE I. Critical exponents for FeF_2.

Exponent	Value	Theory Method[a]	Reference	Value	Experiment Method[a]	Reference
α	0.109(5)	RG	(6)	0.111(7)	SH	(16)
				0.115(4)	LMB	(16)
β	0.3250(20)	RG	(6)	0.325(5)	MS	(17)
				0.331(6)	NMR	(18)
γ	1.2410(20)	RG	(6)	1.38(8)	NS	(20)
				1.25(2)	NS	(21)
ν	0.6300(15)	RG	(6)	0.67(4)	NS	(20)
				0.64(1)	NS	(21)
z	2.173(5)	DS	(22)	2.09(4)	NMR	(19)
				2.1(2)	NS	(20)

[a]Abbreviations for methods used are as follows: DS, dynamical scaling; LMB, linear magnetic birefringence; MS, Mössbauer spectroscopy; NMR, nuclear magnetic resonance; NS, neutron scattering; RG, renormalization group; SH, specific heat.

B. Sample preparation

Single crystals of $Fe_{0.9}Zn_{0.1}F_2$ were grown by Guggenheim from a stoichiometric mixture of FeF_2 and ZnF_2 powders using a horizontal-zone method. The FeF_2 was prepared by reacting a high-purity 99.999% Fe sponge with dry HF at 900 C. ZnF_2 was made in a similar way. The composition quoted was obtained by x-ray fluorescence and chemical analysis of a sample cut from the same batch. The principal data were taken with a $4\times5\times0.1$-mm^3 polished {001} platelet mounted in a strain-free manner as described above.

C. Minimizing concentration gradients

An overriding consideration for good critical-phenomena studies is eliminating the effects of macroscopic concentration gradients, which can cause T_c rounding. One approach is to choose a concentration for which $dT_c/dx=0$.[24,25] Another is to choose a sample geometry which minimizes the effect of the gradient. Since the first method is unavailable for $Fe_{1-x}Zn_xF_2$, we were guided by the fact that the largest gradients are usually found along the growth axis.

To check for residual gradients we conducted CVT thermal scans near T_c, with results as shown in Fig. 2. The constant velocity v_0 was chosen so that $+v_0$ coincided with the high-velocity line of the quadrupole doublet above T_c and $-v_0$ sampled the baseline of the spectrum (see Fig. 3).

It is clear from Fig. 2 that for our sample $\Delta T_c \leq 0.025$ K holds, and that this is equivalent to the rounding limit observed for a powder sample of FeF_2. In contrast, a sample with the c axis in the plane of the absorber has much larger rounding. Using $dT_c/dx=-0.75$ K/at. % Zn as deduced from Fig. 2 (this is consistent with Wertheim's value), and assuming that the observed rounding is primarily produced by the gradient in the plane of the absorber, we estimate the gradient to be

$$dx/dl=(dT_c/dl)/(dT_c/dx)=0.1 \text{ at. \% Zn/cm} \quad (2)$$

for the sample with the c axis perpendicular to the plane, and a factor of 5 larger for the sample with the c axis parallel to the plane. This is consistent with recent estimates by King, Ferreira, Jaccarino, and Belanger,[26] who find gradients of 0.5–1.0 at. % Zn/cm along the growth axis, and an order of magnitude less for other directions.

IV. ANALYSIS OF MÖSSBAUER SPECTRA BELOW T_c

For our $Fe_{0.9}Zn_{0.1}F_2$ sample with its c axis perpendicular to the absorber plane we obtained 20 constant-acceleration Mössbauer spectra in the reduced-temperature range $3\times10^{-4}<t<0.86$, with 19 points for $t\leq10^{-1}$. Here $t\equiv1-T/T_c$ is the reduced temperature. Because the direction of the γ rays is parallel to the c axis the $\Delta m=0$ lines are suppressed, and the strongly asymmetric spectra have four lines at low temperature. As the

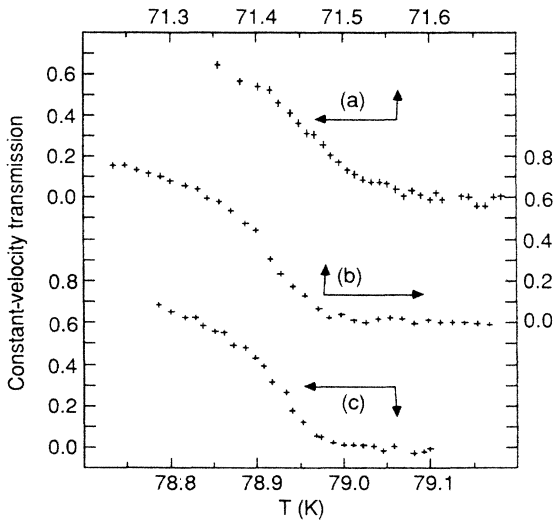

FIG. 2. Constant velocity thermal scans for (a) $Fe_{0.9}Zn_{0.1}F_2$ with the growth axis in the absorber plane, (b) $Fe_{0.9}Zn_{0.1}F_2$ with the growth axis perpendicular to absorber plane, and (c) FeF_2 powder. Note that the powder and "perpendicular" sample are equally sharp, whereas the "in-plane" scan is much more rounded.

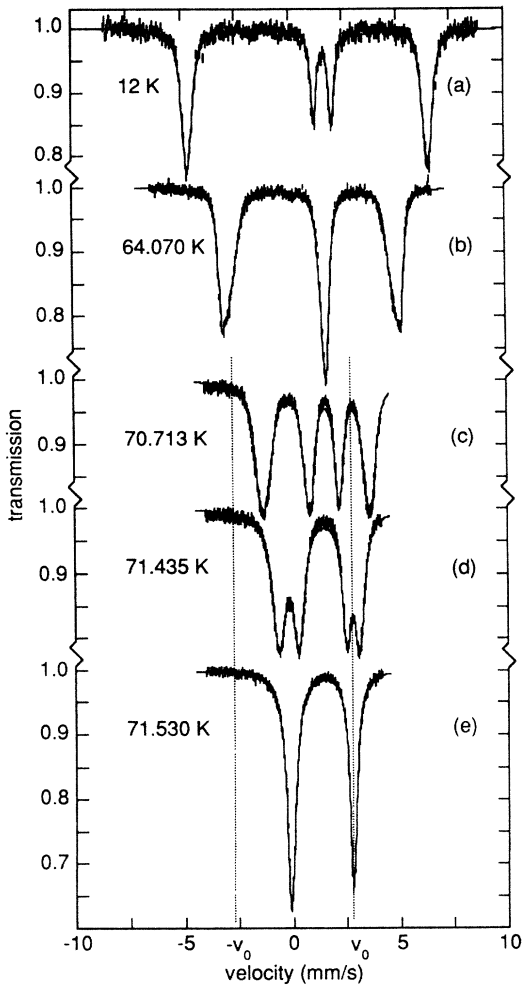

FIG. 3. Mössbauer spectra for a $Fe_{0.9}Zn_{0.1}F_2$ single crystal with the c axis, growth axis, and γ rays perpendicular to the absorber plane. Spectra (a)–(d) are below T_c, and are fit via a four-site diagonalized Hamiltonian procedure, as described in the text. Spectrum (e) is above T_c, and is fit via two independent Lorentzian lines. The velocities $\pm v_0$ indicate the values used for thermal scans.

magnetic splitting decreases, the inner lines cross at $t \approx 0.1$, until, as t approaches zero, the inner and outer lines merge and the magnetic interaction is reduced to line broadening of the quadrupole doublet. This entire sequence of spectral change is illustrated in Fig. 3.

Just below T_c, in the region $t \leq 10^{-3}$, a 2% paramagnetic component is visible as a fifth line. Similarly, just above T_c, in the region $t \leq 10^{-3}$ the quadrupole lines exhibit small deviations from Lorentzian shape which may be interpreted as a $\sim 5\%$ admixture of the antiferromagnetic phase. Neither minority phase is recognizable in the CVT scans of Fig. 2. We believe, therefore, that the presence of minority phases is justifiably neglected in the analysis of critical behavior.

Extracting $H_{\rm hf}(T)$ from the data requires solving the combined interaction Hamiltonian

$$\mathcal{H} = -g\mu_N H_{\rm hf} \mathbf{I}_{z'} + e^2 q_{zz} Q [3\mathbf{I}_z^2 - I(I+1) + \eta(\mathbf{I}_x^2 - \mathbf{I}_y^2)]/[4I(2I-1)] , \quad (3)$$

where the angular momentum operators $\mathbf{I}_{z'}$ and $\mathbf{I}_z$ are defined with respect to two different coordinate systems, suitable, respectively, for representing the magnetic and quadrupole interaction in diagonal form. The coordinates x,y,z represent the principal axes of the EFG tensor, z' is the direction of the hyperfine field, $g\mu_N H_{\rm hf}$ and $e^2 q_{zz} Q/2$ are the magnetic and quadrupole interaction strength, and $\eta = (q_{xx} - q_{yy})/q_{zz}$ is the asymmetry parameter.

To gain an appreciation of the problems of data analysis, and to permit a direct comparison to the work of Barrett,[11] we present three increasingly realistic ways of fitting the Mössbauer spectra and deriving $H_{\rm hf}(T)$.

A. Line subtraction

If $H_{\rm hf}$ is aligned along one of the principal axes of the EFG tensor the $I = \frac{3}{2}$ state of ^{57}Fe has energy eigenvalues

$$E_{1,3} = g_e \mu_N H_{\rm hf}/2 \pm \tfrac{1}{4} e^2 Q q_{zz} \{[1 + (4 g_e \mu_N H_{\rm hf}/e^2 Q q_{zz})]^2 + \eta^2/3\}^{1/2} , \quad (4a)$$

$$E_{2,4} = -g_e \mu_N H_{\rm hf}/2 \pm \tfrac{1}{4} e^2 Q q_{zz} \{[1 - (4 g_e \mu_N H_{\rm hf}/e^2 Q q_{zz})]^2 + \eta^2/3\}^{1/2} , \quad (4b)$$

where $g_e \mu_N$ is the excited-state moment. In this case one may write the energies of the four $\Delta m = \pm 1$ Mössbauer lines as

$$E_a = E_0 + E_2 - g_g \mu_N H_{\rm hf}/2 , \quad (5a)$$

$$E_b = E_0 + E_1 + g_g \mu_N H_{\rm hf}/2 , \quad (5b)$$

$$E_c = E_0 + E_4 - g_g \mu_N H_{\rm hf}/2 , \quad (5c)$$

$$E_d = E_0 + E_3 + g_g \mu_N H_{\rm hf}/2 , \quad (5d)$$

where E_0 is the unperturbed energy difference between the nuclear excited and ground state, and $g_g \mu_N$ is the ground-state moment. This leads directly to the closed expression

$$H_{\rm hf} = [(E_c - E_d) + (E_a - E_b)]/2(g_e - g_g)\mu_N , \quad (6)$$

which can be used to extract $H_{\rm hf}$ from fitted line positions.

As the simplest form of data analysis, and one that is similar to Barrett's,[11] we fitted the spectra with four independent Lorentzians and employed Eq. (6) to extract $H_{\rm hf}(T)$. This requires that $H_{\rm hf}$ be aligned along one of the principal axes of the EFG, as assumed in Eqs. (4). For FeF_2 Wertheim[17] proved this by explicit diagonalization at 4.2 K, but there is no reason to assume it *a priori* at other temperatures.

The use of Eq. (6) has other problems. As illustrated in Fig. 4(a), the spectra for $t > 2 \times 10^{-3}$ are poorly fit be-

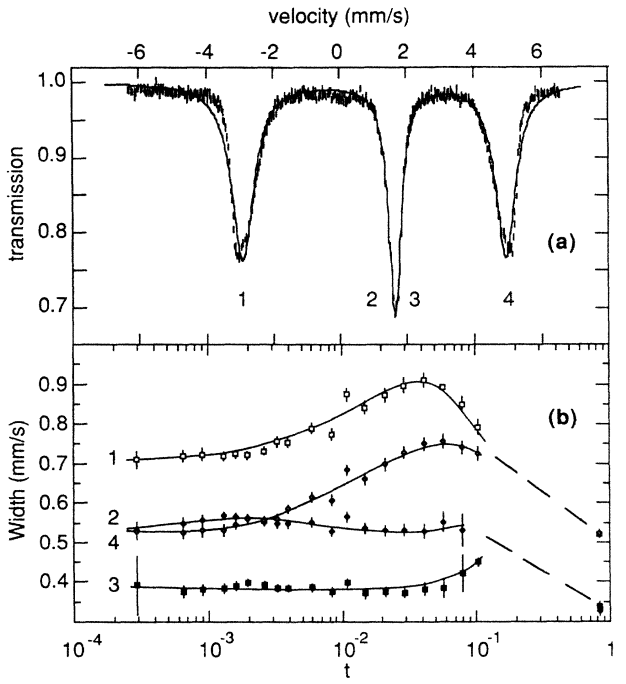

FIG. 4. Results of fitting using four independent Lorentzian lines: (a) spectrum for $t=0.1$; (b) temperature dependence of linewidths below T_c. The lines are numbered in the order of increasing energy.

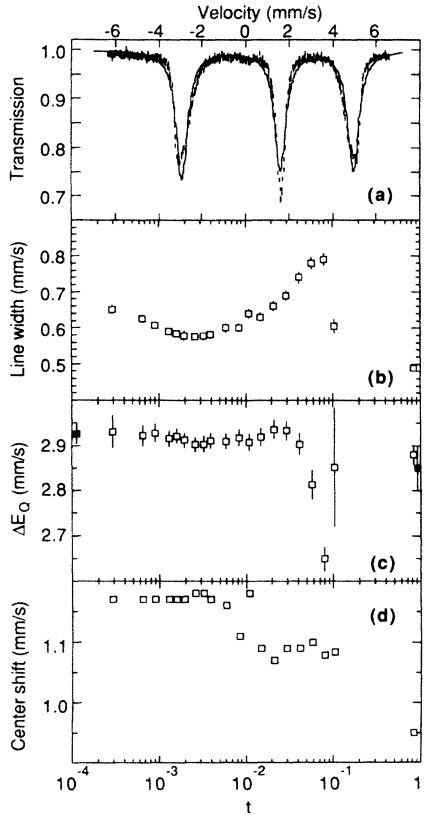

FIG. 5. Results of fitting using a single-site diagonalized Hamiltonian: (a) spectrum for $t=0.1$; (b) temperature dependence of linewidth below T_c; (c) quadrupole splitting, $\Delta E_Q=(e^2q_{zz}Q/2)(1+\eta^2/3)^{1/2}$; and (d) center shift below T_c, indicating our data via open symbols, and those of previous workers (see Refs. 14, 17, 23, and 28) via closed symbols. The large errors in the quadrupole splitting near $t=0.1$ arise from line crossing. The misfit of the spectrum and the variation of the center shift are attributed to the inadequacy of the spectral fitting procedures.

cause a single Lorentzian cannot capture the asymmetric line shape or the variable linewidth produced by inhomogeneous broadening. One consequence of this, illustrated in Fig. 4(b), is that there is *no linewidth anomaly* for $t<10^{-2}$, as one would expect based on critical fluctuation broadening for $T>T_c$ (see Sec. VI). We can explain this qualitatively by the fortuitous cancellation of declining inhomogeneous broadening and increasing dynamical broadening.

B. Diagonalized Hamiltonian fit for a single site

As a second approach we adapted a computer program developed by Kündig's group[27] which numerically diagonalizes the Hamiltonian of Eq. (3). This constrains line positions and intensities, and allows us to check whether the relative orientation of H_{hf} and the EFG are independent of T, as assumed in Eq. (6).

The diagonalization program has six free parameters: the baseline, center shift, linewidth, total absorption, total magnetic splitting, and the ratio of the magnetic to the quadrupole energy. The parameter η, the angles defining the geometry of H_{hf}, the EFG, and the γ ray are fixed. The latter include the polar and azimuthal angles θ_I and ϕ_I defining the orientation of $\mathbf{I}_{z'}$ with respect to $\mathbf{I}_z$, and the polar and azimuthal angles θ_γ and ϕ_γ defining the orientation of the γ ray with respect to $\mathbf{I}_z$.

The best fits were obtained for $\theta_I=90°$, $\phi_I=0°$, $\theta_\gamma=90°$, $\phi_\gamma=0°$, and $\eta=0.4$, independent of temperature. Since these values are the same as presupposed in the derivation of Eqs. (4)–(6), and determined previously[17] at 4.2 K, they justify the method of the previous section. These results are summarized in Fig. 5 and indicate there is now a weak linewidth anomaly as $T\rightarrow T_c^-$ and the fitted quadrupole interaction agrees with previous results at $T=4.2$ and 80 K.[14,17,28]

The principal problem with single-site diagonalization is that the line shape and line intensity both fit poorly, and the center shift exhibits an unreasonably strong temperature dependence, far in excess of theoretical expectations for the isomer and second-order Doppler shifts. We attribute these problems to the fact that inhomogeneous broadening and line saturation were not considered.

C. Diagonalized Hamiltonian fit for four magnetic sites

Neutron spin-wave studies[29] indicate that in FeF_2 the strongest magnetic coupling is between next-nearest-neighbor Fe atoms. We therefore model the local environment reflected in our Mössbauer spectra by considering only the eight next nearest Zn or Fe neighbors as determinants of H_{hf} in $Fe_{0.9}Zn_{0.1}F_2$. Assuming that this produces hyperfine field shifts that are linear with respect

to the number of Zn neighbors, n, we decompose H_{hf} into four components:

$$H_n = H_0(1 + n\Delta h), \quad n = 0,1,2,3 , \tag{7}$$

where H_0 is the hyperfine field for zero Zn neighbors, and Δh is a dimensionless shift parameter.

To incorporate this model into our fitting procedure, we extended the numerical diagonalization program to four magnetic sites. The quadrupole splitting and center shift were assumed to be independent of the local Zn configuration.[23] The line intensities and positions were again constrained by the ratio of magnetic to quadrupole splitting and by the relative orientation of the magnetic easy axis, the EFG, and the γ rays. By fitting the spectrum with the best-resolved local environment structure (this occurs at $T \approx 64$ K), the intensity distribution of assumed site configurations was found to be close to random, although there is evidence for small residual short-range order as shown in Fig. 6.

The results of fitting are summarized in Fig. 7. Figure 7(a) shows we now obtain good fits for $t > 10^{-2}$, where neither of the other methods was successful. In Figs. 7(b) and 7(c) the quadrupole interaction is consistent with previous work[14,17,28] and the center shift is constant to within 0.01 mm/s (the long-term stability of the drive). Figure 7(d) indicates that $1+\Delta h$ ranges from 0.98 at $t = 0.86$ to 0.85 at $t = 10^{-2}$. The result at 12 K is consistent with Wertheim's observation.[23] The temperature dependence of $1+\Delta h$ is noted here for the first time in Zn diluted FeF_2, and is comparable to effects observed in Fe alloys.[30] Figure 7(e) shows that site-component linewidths have complex behavior which can be explained in the following three parts.

(i) For $t > 10^{-1}$ the outer linewidths decrease and the inner linewidths increase. Both are due to saturation effects. For the outer lines the increase in Δh *decreases* the overlap of the site components, and hence *decreases* line saturation broadening. For the inner lines the combined interaction moves them toward each other (they eventually cross), and this *increases* line overlap, and hence line saturation broadening.

(ii) For $10^{-1} < t < 5\times10^{-3}$ the outer linewidths increase rapidly and the inner linewidths increase slowly. This is explained by the rapid decline of H_{hf}, which overwhelms the increase in Δh and increases overlap, and hence the degree of saturation broadening.

(iii) For $t < 5\times10^{-3}$ the linewidth increases rapidly; this is explained by the addition of dynamical broadening to the effects of increasing site-component overlap.

Whereas multisite diagonalization obviously provides a much more satisfactory analysis of the Mössbauer spectra than either line subtraction or single-site diagonalization, a problem remains. For $t < 2\times10^{-3}$ it is difficult to fit a unique value of Δh. This is because it is impossible to distinguish between inhomogeneous broadening, which produces *asymmetrical* line shapes, and dynamical effects

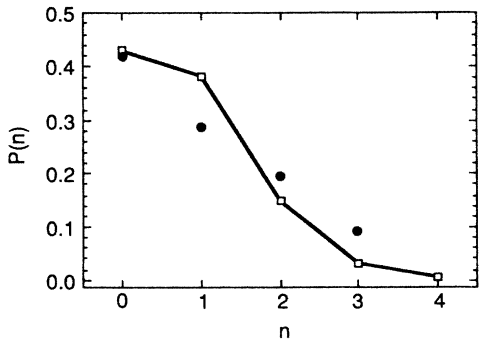

FIG. 6. Distribution function for the number n of Zn nearest neighbors, with experimental data indicated via closed symbols and the binomial distribution via open symbols.

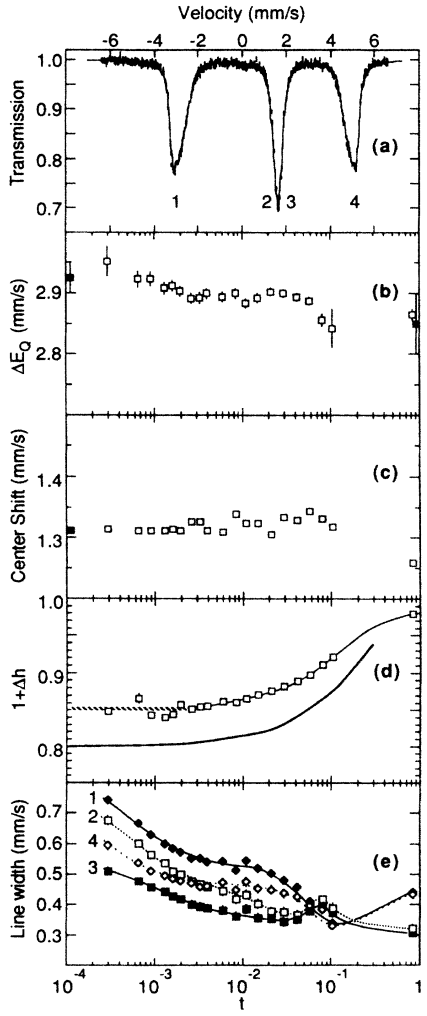

FIG. 7. Results of fitting using multiple-site diagonalized Hamiltonian: (a) spectrum for $t = 0.1$ with lines numbered in order of increasing energy; (b) quadrupole splitting, $\Delta E_Q = (e^2 q_{zz} Q/2)(1+\eta^2/3)^{1/2}$; and (c) center shift below T_c, indicating our data via open symbols, and those of previous workers (see Refs. 14, 17, 23, and 28) via closed symbols; (d) temperature dependence of $1+\Delta h$, with the dashed line indicating the region in which $1+\Delta h$ was fixed, and the heavy line the calculation of Bergstresser and Gould (Ref. 31); (e) linewidths below T_c. Note that the spectrum, the quadrupole interaction, the center shift, and $1+\Delta h$ are all well fit. The behavior of the linewidths is discussed in the text.

which lead to *symmetrical* line broadening. To solve this problem, we note that the temperature variation of Δh must be a phenomenon that only occurs *outside* the asymptotic critical region, where magnetic correlations are of the order of interatomic distances. Close to T_c the existence of long-range correlations demand that all site components have the same relative temperature dependence.

In support of this assumption, we compare our data to theoretical work by Bergstresser and Gould,[31] who considered a magnetic atom with a single diamagnetic neighbor in the $d=3$ Ising model. They obtained $\sigma_1(t)$, the moment on the disturbed magnetic atom, and compared it to $\sigma_0(t)$, the moment on an undisturbed magnetic atom. As indicated by the solid curve in Figure 7(d), the calculated moment disturbance has a temperature dependence similar to our data for $1+\Delta h$: it is strongly temperature dependent for $t>10^{-2}$, and becomes essentially temperature independent for $t<10^{-2}$.

Guided by this, we treated Δh as free for $t>3\times10^{-3}$, fixed it at -0.15 for $t<3\times10^{-3}$, and used this to obtain the "best" multisite diagonalized Hamiltonian fits of our spectra.

V. THE CRITICAL EXPONENT β

Table II shows the results of the three methods of spectral analysis we have described. To extract β we made a nonlinear least squares fit of the reduced hyperfine fields to the expression

$$h(t)=Bt^{\beta}(1+at^{\Delta}) , \tag{8}$$

where Bt^{β} is the usual asymptotic singular term, at^{Δ} describes corrections to scaling with $\Delta=0.50$ fixed at its theoretical value,[6] and T_c, B, a, and β are free.

Since site components exhibit the most significant differences in the range $t>10^{-2}$, the largest differences between methods of spectral analysis occur in the fitted correction-to-scaling amplitude a as illustrated in Table III. In addition, the three methods of spectral analysis show substantially different values β and B.

Since multisite diagonalization has been demonstrated to be the most reliable spectral fitting procedure, we regard critical parameters deduced from the hyperfine fields obtained by this method (Table III, line 3) as the most reliable. The quality of fit obtained with these values is illustrated in Fig. 8 via a logarithmic plot of $h(t)$. The result $\beta=0.350(9)$ is in good agreement with the most recent theoretical predictions,[7] according to which $\beta=0.3494(15)$ for $d=3$ random Ising model.

As a check on the critical-parameter fitting procedure we made a "range-of-fit analysis," as described in earlier work by our group.[32,33] In this method, data with a reduced temperature $t<t_{\max}$ are fitted by the simple power law $h=Bt^{\beta}$, with β, T_c, and B free. As shown in Fig. 9, by plotting these parameters against $t_{\max}$, one may directly observe the approach to asymptotic values, albeit with increasing error as the range of fit is reduced. Evidently, the results of this procedure are consistent with the least squares fit to Eq. (8).

Our results may be compared to the MS work of Barrett,[11] who in a study of powder samples of $Fe_{1-x}Zn_xF_2$, for $0.01<x<0.54$, derived average values of $H_{\rm hf}(T)$ via line subtraction, and for $x<0.07$ found a concentration-dependent crossover from $\beta=0.33$ to $\beta=0.36$ as $T\rightarrow T_c^-$. We can draw no direct conclusions about cross-

TABLE II. Hyperfine fields deduced by three methods of analysis.

T (K)	$\langle H_{\rm hf}(T)\rangle$ (kG) line subtraction	$\langle H_{\rm hf}(T)\rangle$ (kG) single-site diagonalization	$H_0(t)$ (kG) multisite diagonalization	Δh[a] multisite diagonalization
12.5	320.76(9)	321.8(4)	328.0(2)	−0.021(1)
64.070	210.34(15)	209.2(25)	222.6(6)	−0.078(1)
65.841	190.23(57)	197.44(55)	206.3(2)	−0.090(1)
67.389	171.58(20)	175.01(65)	187.8(2)	−0.103(1)
68.554	153.24(17)	154.38(52)	169.6(2)	−0.111(1)
69.402	136.54(17)	136.78(49)	152.5(2)	−0.118(1)
70.009	121.41(17)	121.52(46)	136.7(2)	−0.124(1)
70.425	107.11(16)	107.11(42)	121.5(2)	−0.129(1)
70.713	94.36(11)	94.17(37)	107.5(2)	−0.134(1)
70.893	86.64(16)	86.76(35)	99.6(2)	−0.139(1)
71.079	78.04(11)	77.86(31)	89.4(2)	−0.138(2)
71.220	67.95(11)	67.74(28)	78.5(2)	−0.145(2)
71.266	62.94(11)	62.79(27)	72.9(2)	−0.146(2)
71.313	57.72(11)	57.61(24)	67.2(2)	−0.149(2)
71.360	52.42(11)	52.30(23)	61.2(2)	[−0.149]
71.386	50.11(15)	49.61(22)	58.0(2)	[−0.149]
71.407	45.54(20)	44.59(21)	52.2(2)	[−0.149]
71.435	42.06(22)	40.01(22)	47.0(2)	[−0.149]
71.453	39.32(32)	35.65(23)	42.1(2)	[−0.149]
71.479	35.10(65)	25.59(28)	30.1(2)	[−0.149]

[a]Square brackets [ ] indicate the parameter Δh has been fixed as described in the text.

TABLE III. Fitted critical parameters. Our most reliable values for the critical parameters are determined from hyperfine fields calculated via the four-site diagonalization procedure (as described in the text).

Method of analysis	T_c	B	β	a
line subtraction	71.515(10)	1.55(12)	0.369(14)	−0.17(15)
one-site diagonalization	71.496(3)	1.27(8)	0.334(10)	0.36(15)
four-site diagonalization	71.498(3)	1.68(8)	0.350(9)	−0.32(8)

over in the exponent β as observed by Barrett, since we have no data in the region $x < 0.07$. However, from our analysis we can make the following three comments about Barrett's work.

(1) We have shown that a four-site analysis of inhomogeneous broadening gives the best fit to our line shape, and yields significantly different critical behavior than less sophisticated forms of analysis. This means that explicit consideration of inhomogeneous broadening is *needed* at $x = 0.10$, as well as over some part of the range $x < 0.10$. Hence Barrett's conclusion for the range $x < 0.07$ probably should be reexamined.

(2) In the region $x \approx 0.5$ we know that inhomogeneous broadening is a major factor, but our method of multisite analysis would be hopelessly complex. It is, therefore, unclear to us how to deal with inhomogeneous broadening near $x = 0.5$ and how to evaluate Barrett's dynamic or static data in this region.

(3) Independent of spectral analysis, we note that Barrett's power-law fitting makes no corrections to scaling and is sensitive to the stated error in T_c. It is therefore possible that crossover in β is related to corrections to scaling or the particular choice of T_c. (See Fig. 10).

Our work may also be compared to the NMR study of $Mn_{0.87}Zn_{0.13}F_2$ by Dunlap and Gottlieb.[10] Whereas this yielded $\beta = 0.349(8)$, in agreement with theory and the present work, it employed an irregularly shaped 0.4-g single crystal which was analyzed for neither concentration gradients nor hyperfine field inhomogeneity.

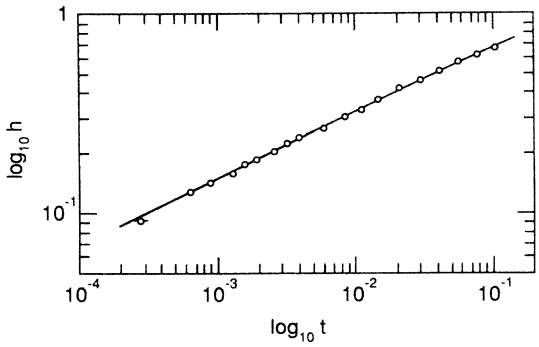

FIG. 8. Log-log plot of reduced hyperfine field vs reduced temperature. The line is a fit to the data of the form $Bt^{\beta}(1+at^{\Delta})$ with $B = 1.68(8)$, $\beta = 0.350(9)$, $a = -0.32(10)$, and $\Delta \equiv 0.5$.

VI. CRITICAL DYNAMICS

In contrast to pure FeF_2, where no effect was found,[17] line broadening for $Fe_{0.9}Zn_{0.1}F_2$ in the region $10^{-4} < t < 10^{-1}$ above T_c is clearly visible. We attribute the observed broadening to critical fluctuations. As indicated in Fig. 11, broadening is larger for the $I_e = \pm\frac{1}{2}$ to $I_g = \pm\frac{1}{2}$ quadrupole line than the $I_e = \pm\frac{3}{2}$ to $I_g = \pm\frac{1}{2}$ line. According to Blume and Tjon,[34] this is to be expected for the case in which magnetic fluctuations are transverse to the principal component of the EFG, as is the case in the FeF_2 system. At the same time, the observed effect is inconsistent with isotropic fluctuations as discussed by Bradford and Marshall.[35]

Because the observed line broadening is less than the

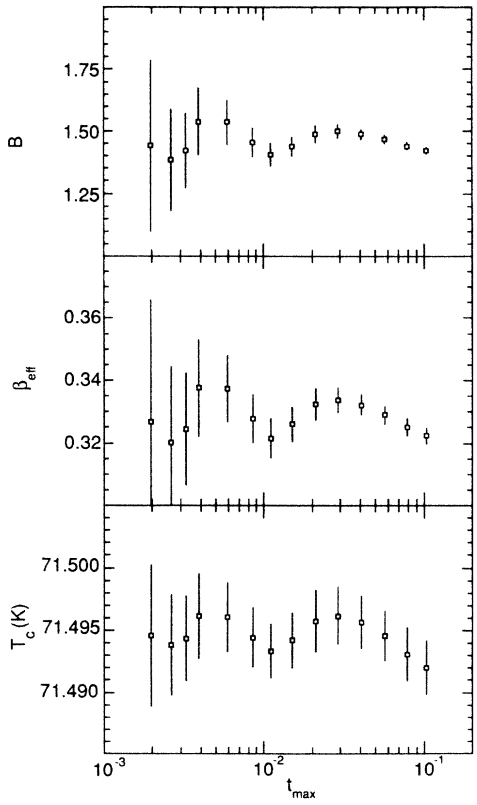

FIG. 9. Range of fit analysis for reduced hyperfine field. The temperature t_{max} indicates the maximum value of t included in the fit to $h(t) = Bt^{\beta}$.

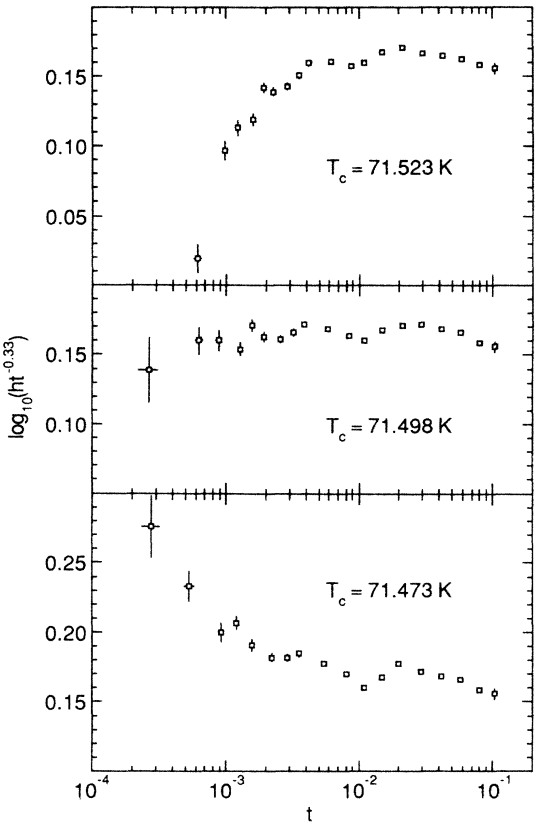

FIG. 10. Plots of $\log_{10}(ht^{-0.33})$ vs t for three values of T_c, using the data given in Table III. The values of T_c span one half of the error quoted in Ref. 11. This indicates the great sensitivity of "crossover" to the choice of T_c.

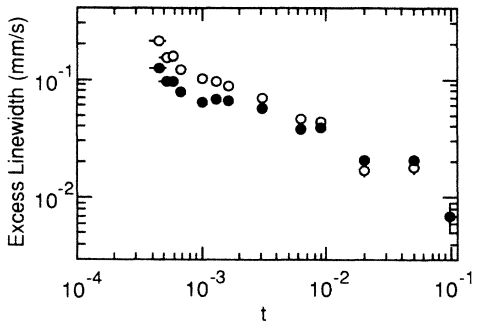

FIG. 11. Critical line broadening above T_c. Open circles indicate the $I_e = \pm\frac{1}{2} \rightarrow I_g = \pm\frac{1}{2}$ transition; closed circles indicate the $I_e = \pm\frac{3}{3} \rightarrow I_g = \pm\frac{1}{2}$ transition.

natural linewidth at all temperatures, we believe we are sampling the extreme "motional narrowing" regime. In this case much of the spectral complexity described by Blume and Tjon[34] disappears. Nevertheless, the observed line width anomaly is subject to at least two interpretational difficulties.

(1) The presence of four major components in the magnetically ordered spectra means the line broadening above T_c will have four components, each with a different amplitude of the fluctuating hyperfine field.

(2) Because the recoilless fraction changes noticeably in the range $t \leq 10^{-1}$ above T_c, critical line broadening will be confounded by changes in line saturation, particularly for relatively thick absorbers such as ours, with 40% absorption dips above T_c.

For these reasons we have *not* interpreted our present data (Fig. 11) in terms of a dynamical critical exponent, but are planning further experiments and analysis to be reported elsewhere.

VII. SUMMARY AND CONCLUSION

Using a single-crystal sample of $Fe_{0.9}Zn_{0.1}F_2$ for which a study of T_c rounding demonstrates that the effect of concentration gradients is negligible, we have shown via Mössbauer spectroscopy that the order parameter is described by the critical exponent $\beta = 0.350(9)$. This value for β is consistent with the most recent theoretical predictions for the $d = 3$ REIM. Our result applies in the range $3 \times 10^{-4} < t < 10^{-1}$ with substantial corrections to scaling for $t > 10^{-2}$. Our analysis of spectra below T_c makes clear that for a sample with as little as 10% Zn dilution a multisite diagonalization procedure is necessary to account adequately for the line shapes produced by different local environments.

It is interesting that none of the experiments on the exponent β in the REIM show evidence of the *slow crossover* predicted by Newman and Riedel,[36] who obtain a crossover exponent of $1/\alpha$ and a RE asymptotic region of $t < 10^{-9}$. In fact, except for the *rapid crossover* for $x < 0.07$ reported by Barrett,[11] only the predicted REIM β values are observed, without crossover of any kind. This is clearly an unresolved discrepancy between theory and experiment which requires further work.

Above T_c we observed substantial line broadening, which we attribute to critical fluctuations. However, the presence of both hyperfine field inhomogeneity and line saturation effects argues against deduction of an exponent. We have therefore deferred this issue.

Note added in proof. Recently, Thurston *et al.*[37] have performed magnetic x-ray measurements on another REIM system, $Mn_{0.5}Zn_{0.5}F_2$, which yield $\beta = 0.33(2)$ over the reduced temperature range $0.001 < t < 0.06$. They correctly point out that thier result for β if consistent with ours. They also wonder whether choosing a correction to scaling exponent of $\Delta = \alpha = 0.11$ would change our value of β. Reanalysis of our data shows this choice does not alter β; correction to scaling analysis with $\Delta = 0.11$ yields $\beta = 0.35(1)$ as before.

ACKNOWLEDGMENTS

We thank H. J. Guggenheim for making the high quality samples used in this work. We acknowledge helpful discussions during the course of this work with X. S. Chang, G. S. Collins and R. Schuhmann. Research support of the work done at Clark University was received from the National Science Foundation under Grant No. DMR 8303611.

[1]Y. Imry and S. Ma, Phys. Rev. Lett. **35**, 1399 (1975).
[2]S. Fishman and A. Aharony, J. Phys. C **12**, L729 (1979).
[3]A. R. King and D. P. Belanger, J. Magn. Magn. Mater. **53**, 5 (1986).
[4]A. B. Harris, J. Phys. C **7**, 1671 (1974).
[5]G. Grinstein and A. Luther, Phys. Rev. B **13**, 1329 (1976).
[6]J. C. LeGuillou and J. Zinn-Justin, Phys. Rev. B **21**, 3976 (1980).
[7]G. Jug, Phys. Rev. B **27**, 609 (1983).
[8]R. J. Birgeneau, R. A. Cowley, G. Shirane, H. Yoshizawa, D. Belanger, A. R. King, and V. Jaccarino, Phys. Rev. B **27**, 6747 (1983).
[9]D. P. Belanger, A. R. King, and V. Jaccarino, Phys. Rev. B **34**, 452 (1986).
[10]R. A. Dunlap and A. M. Gottlieb, Phys. Rev. B **23**, 6106 (1981).
[11]P. H. Barrett, Phys. Rev. B **34**, 3513 (1987).
[12]A. R. Arends, Microprocessorsystems, Noorderwardstraat Noorderwardstraat 1, 9717 LW Groningen, Netherlands.
[13]S. Margulies and J. R. Ehrman, Nucl. Instrum. Methods **12**, 131 (1960).
[14]D. P. Johnson and R. Ingalls, Phys. Rev. B **1**, 1013 (1970).
[15]G. K. Wertheim, Phys. Rev. **121**, 63 (1961).
[16]D. P. Belanger, P. Nordblad, A. R. King, V. Jaccarino, L. Lundgren, and O. Beckman, J. Magn. Magn. Mater. **31-34**, 1095 (1983).
[17]G. K. Wertheim and D. N. E. Buchanan, Phys. Rev. **161**, 478 (1967).
[18]S. M. Kulpa, J. Appl. Phys. **40**, 2274 (1969).
[19]A. M. Gottlieb and P. Heller, Phys. Rev. B **3**, 3615 (1971).
[20]M. T. Hutchings, M. P. Schulhof, and H. J. Guggenheim. Phys. Rev. B **5**, 154 (1971).
[21]D. P. Belanger and H. Yoshizawa, Phys. Rev. B **35**, 4823 (1987).
[22]P. C. Hohenberg and B. I. Halperin, Rev. Mod. Phys. **49**, 435 (1977).
[23]G. K. Wertheim, D. N. E. Buchanan, and H. J. Guggenheim, Phys. Rev. **152**, 527 (1966).
[24]D. P. Belanger, A. R. King, and V. Jaccarino, J. Appl. Phys. **53**, 2704 (1982).
[25]X. S. Chang and C. Hohenemser, Phys. Rev. B (to be published).
[26]A. R. King, I. B. Ferreira, V. Jaccarino, and D. P. Belanger, Phys. Rev. B **37**, 219 (1987).
[27]W. Kündig, Nucl. Instrum. Methods **48**, 219 (1967); **75**, 336 (1969); W. Hofmann, H. Keller, and W. Kündig, *ibid.* **143**, 609 (1977).
[28]U. Ganiel and S. Shtrikman, Phys. Rev. **177**, 503 (1969).
[29]M. T. Hutchings, B. D. Rainford, and H. J. Guggenheim, J. Phys. C **3**, 307 (1970).
[30]F. van der Woude and G. A. Sawatzky, Phys. Rep. **12**, 335 (1974).
[31]T. K. Bergstresser and H. Gould, J. Phys. C **12**, 2611 (1979).
[32]C. Hohenemser, T. Kachnowski, and T. K. Bergstresser, Phys. Rev. B **13**, 3154 (1976).
[33]G. S. Collins, A. R. Chowdhury, and C. Hohenemser, Phys. Rev. B **26**, 4997 (1982).
[34]M. Blume and J. A. Tjon, Phys. Rev. **165**, 446 (1968).
[35]E. Bradford and W. Marshall, Proc. Phys. Soc. London **87**, 731 (1966).
[36]K. E. Newman and E. K. Riedel, Phys. Rev. B **25**, 264 (1982).
[37]T. R. Thurston, C. J. Peters, R. J. Birqeneau, and P. M. Horn (unpublished).

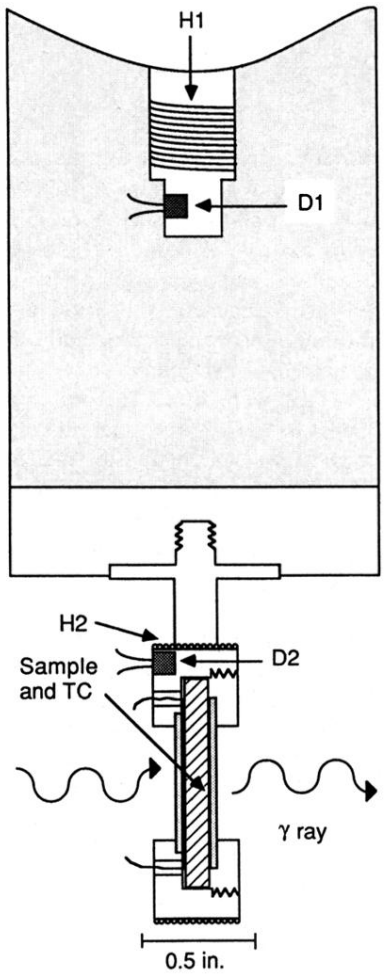

FIG. 1. Cold-finger arrangement with temperature-control system. The primary heater H1 and the diode D1 regulate and measure the temperature of the cold finger connected to the closed-cycle ^{4}He refrigerator. Exchange gas couples the cold finger to the sample holder, which is controlled via a feedback system consisting of the secondary heater H2 and the Si diode D2. A thermocouple TC provides an independent determination of T.